Ga interaction with ZnO surfaces: diffusion and melt-back etching

Tomáš Pejchal[a], Kristýna Bukvišová[a], Stella Vallejos[a,c], Daniel Citterberg[a], Tomáš Šikola[a,b] and Miroslav Kolíbal[a,b,*]

[a] CEITEC BUT, Brno University of Technology, Purkyňova 123, 612 00 Brno, Czech Republic

[b] Institute of Physical Engineering, Brno University of Technology, Technická 2, 616 69 Brno, Czech Republic

[c] Instituto de Microelectrónica de Barcelona (IMB-CNM, CSIC), Campus UAB, 08193 Cerdanyola del Vallès, Barcelona, Spain

[*) corresponding author: kolibal.m@fme.vutbr.cz

Abstract

Despite being technologically very attractive, highly-doped zinc oxide whiskers with precisely defined morphology and doping level are difficult to prepare. Here, as an advancing step towards this goal, we show that pre-annealing of ZnO in oxygen-poor conditions (e.g. high vacuum) encourages a deeper diffusion of Ga into the ZnO crystal lattice in contrast to ZnO pre-annealed in oxygen-rich conditions. We also demonstrate that gallium acts as a reactant causing ZnO etching at diffusion temperatures, contrary to Al-based doping of ZnO systems. This behaviour, being similar to gallium melt-back etching during GaN epitaxy on silicon, has not been observed for ZnO so far and can represent a significant hurdle for the post-growth diffusion doping of ZnO nanostructures. The paper suggests possible ways how to diminish this effect.

1. Introduction

Nanostructures made of transition metal oxides (TMOs) are recognised as ideal building blocks for sensing devices based on localised plasmon resonances (collective oscillations of free electron gas coupled with the electromagnetic field) [1]. The large surface-to-volume ratio of nanostructures increases the sensors' sensitivity. At the same time, the possibility of altering the carrier density in nanostructures by different doping levels may lead to plasmon resonance tuning within the near-IR spectral range, opening access to direct detection of molecular fingerprints [2]. To reach carrier density high enough for accessing the near-IR spectral region, group-III doped TMOs are an attractive choice [3]. Ga-doped ZnO whiskers are a prominent representative of this class of materials, being more stable in comparison with Al-doped ZnO [4]. A natural choice for doping strategy is to introduce dopants during the growth of the whiskers. However, it often results in unexpected growth mode changes [5, 6, 7], thus adding more complexity to the parameter-sensitive nanostructure growth. The post-growth doping techniques developed for planar technology (implantation and diffusion doping) avoid these issues. Hence, a more feasible way is to utilise already existing concepts of ZnO whisker growth and alloy these with the group-III metal in a post-growth step. From this perspective, diffusion-induced doping is the most promising way; however, more in-depth studies are required to fully understand the mechanisms at nanoscale systems [8, 9, 10].

Here, we show that diffusion doping of ZnO whiskers is critically dependent on the pre-annealing conditions of ZnO before the diffusion step. Combining ex-situ and in-situ analyses, we are able to extract the diffusion length of Ga in ZnO whiskers. On top of that, we reveal a mechanism behind the formation of etch pits on the ZnO surface, which is strikingly similar to melt-back etching of silicon by gallium [11, 12].

2. Experimental details

Ensembles of ZnO whiskers were synthesised via an aerosol-assisted CVD method (AACVD) at atmospheric pressure. The whiskers were grown via the vapour–solid (VS) mechanism at 400 °C on a silicon wafer; the growth details have already been described elsewhere [13]. The whiskers exhibit six $\{10\bar{1}0\}$-oriented sidewalls and the top (0001)-oriented facet. HCl-based etching experiments [14] have identified that the top facet is O-polar, whereas the sidewalls are non-polar.

For diffusion doping experiments, the ZnO samples were modified either by annealing in vacuum (O-poor conditions) or in H_2O_2 vapour (O-rich conditions). The H_2O_2 oxidative agent has been chosen because (i) it provides a lower concentration of oxygen vacancies (V_O) compared to annealing in O_2, and (ii) it is more reactive than molecular oxygen [15]. The H_2O_2 vapour was supplied via a needle valve from a stainless-steel container held at constant temperature (22 °C). The annealing was performed in a high-vacuum chamber ($p_{base} < 3 \cdot 10^{-6}$ Pa) using a pyrolytic boron nitride heating element, previously calibrated by a thermocouple and a pyrometer [16]. The annealed samples were subsequently transferred under high-vacuum conditions to an interconnected chamber, where the Ga deposition took place. The deposition was carried out from an effusion cell (MBE-Komponenten) at a typical operating pressure of $5 \cdot 10^{-6}$ Pa and evaporation rate 1.1 nm·min^{-1} (calibrated before the experiment using a crystal quartz thickness monitor placed perpendicularly to the Ga flux). After the Ga deposition, the samples were transferred back to the annealing chamber and annealed at the desired temperature for different times to promote Ga diffusion. To monitor the diffusion process in-situ, two different vacuum systems were used. First, an ultrahigh vacuum chamber (UHV, $p_{base} < 3 \cdot 10^{-7}$ Pa) coupled with a scanning Auger microscope system (SAM, Omicron) was used for in-vacuum annealing, Ga deposition and in-situ analysis by real-time scanning electron microscope (SEM) [16]. Second, an in-situ X-ray photoelectron spectroscopy (XPS) measurement was conducted in a complex ultra-high vacuum system, where all the process

steps (annealing, Ga deposition, analysis) can be performed as well. Further, the samples were examined ex-situ with high-resolution SEM (ThermoFisher Verios 460L), XPS (Kratos Analytical Axis Supra) and TEM (ThermoFisher Titan Themis 60-300). The details of XPS sample analysis and peak fitting can be found in the Supplementary information. To investigate gallium diffusion into ZnO whiskers, selected samples were subject to energy-dispersive X-ray spectroscopy (EDS) analysis. For such measurements, <150 nm thick lamellae were made out of the whiskers with a xenon-plasma focused ion beam (ThermoFisher Helios 5 PFIB DualBeam) to avoid Ga implantation from a standard Ga FIB.

3. Results
### 3.1 Characterisation of as-grown and annealed whiskers

The annealing of ZnO in different environments results in the formation of several types of defects [17]. Zinc vacancies are more likely formed during annealing in the oxygen-rich environment and are mobile at relatively low temperatures (270 °C). In contrast, oxygen vacancies are formed during in-vacuum annealing at higher temperatures. The latter procedure has been reported to promote the carrier concentration in Al-doped ZnO [18], and there are indications that it may significantly improve the Ga diffusion into ZnO [19]. Here, to inspect the effect of oxygen vacancies on the Ga diffusion, we have annealed the ZnO whiskers in vacuum ($4 \cdot 10^{-6}$ Pa) and in H_2O_2 atmosphere (6 kPa) at 300 °C or 400 °C, according to the analysis run. The annealing temperature was chosen high enough to promote oxygen vacancy formation (and to maximise the difference between the two kinds of samples) while keeping ZnO below the decomposition temperature (see Fig. 1). Further annealing experiments at 535 °C in high vacuum (i.e., the conditions used for Ga diffusion step) corroborated the stability of the nanorods by displaying stable sidewalls and no signs of decomposition (Fig. 1c,d). The XPS spectra of the samples exhibit mild differences in the O 1s peak (Fig. 1b) at around 531 eV. It is commonly accepted that the O 1s peak contains a relevant component (a peak

deconvolution is not shown here for clarity) that represents the fingerprint of V_O in metal oxides [20]. This interpretation has been questioned quite recently [21], based on the fact that there exists an overlap with a peak component related to hydroxyls. Despite the ongoing debate on the physical origin of this signal, our measurements show a decrease in intensity of this component upon annealing in the oxygen-rich environment, in agreement with other studies where the change of V_O concentration was proved also by other means [17, 22]. In further text, the two distinctly pre-annealed samples will be referred to as V_O-rich (ZnO annealed in high vacuum, resulting in a higher concentration of V_O) and V_O-poor (ZnO annealed in H_2O_2, resulting in low concentration of V_O).
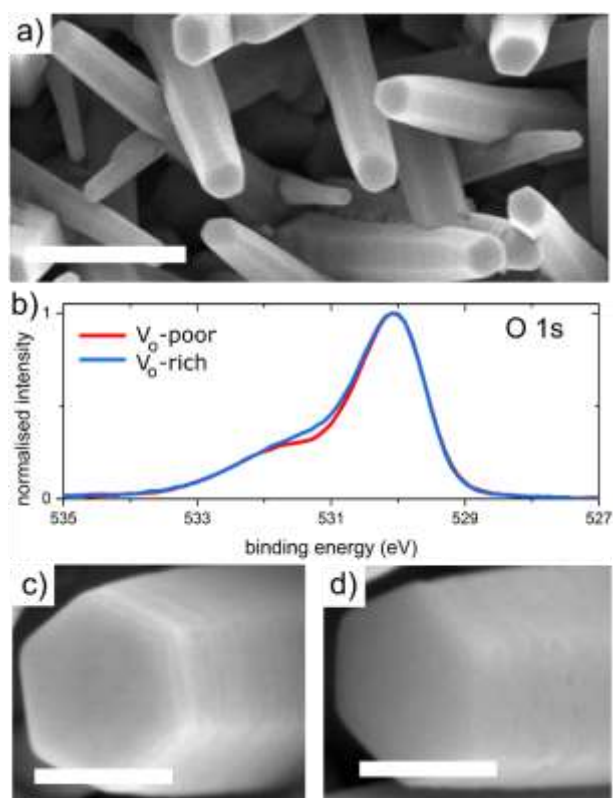
Fig. 1: Characterisation of ZnO whiskers before and after annealing under different pressure conditions. (a) SEM image of the as-grown whiskers. b) O 1s XPS peak measured after pre-annealing at 400 °C in high vacuum ($4 \cdot 10^{-6}$ Pa, blue) and in H_2O_2 atmosphere (6 kPa, red). In both cases, this treatment does not result in any visible changes in morphology. This is shown in c) for a sample treated in H_2O_2 and in d), where the sample from c) was additionally annealed in vacuum for further 30 minutes at 535 °C as a control experiment for the Ga diffusion step. Again, surface morphology remains intact. The scale bar in a) is 500 nm; in c,d) it is 200 nm.
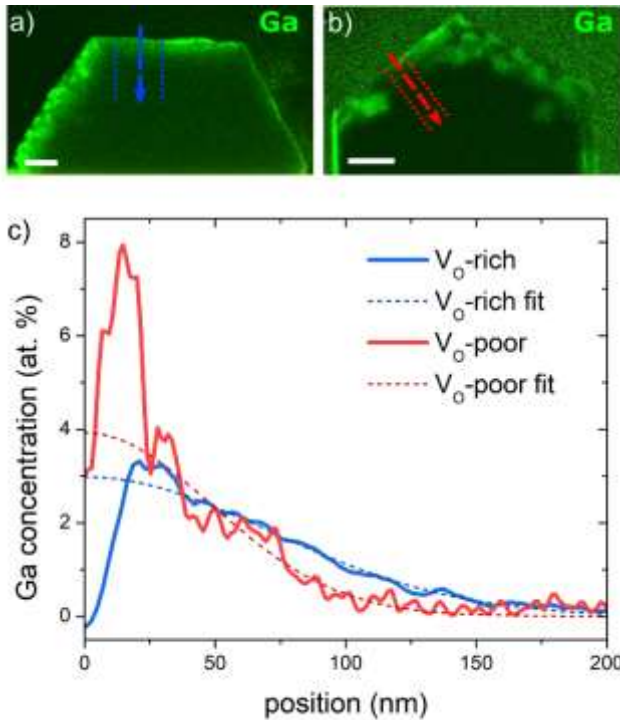
3.2 Ga-diffused whiskers – Ga diffusion
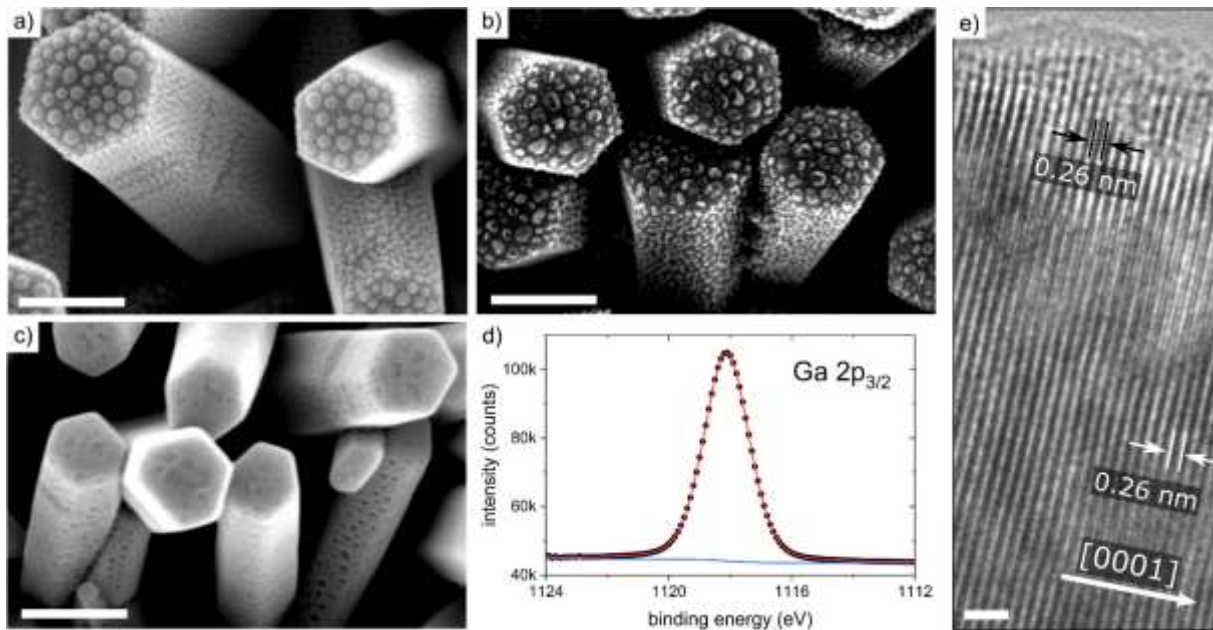
Fig. 2: Morphology, structure and chemical composition of the H_2O_2-preannealed ZnO whiskers after Ga diffusion doping. a) ZnO whiskers after evaporation of nominal thickness of 12 nm of gallium at room temperature. No post-annealing was applied. b) ZnO whiskers after 12 nm Ga deposition and subsequent annealing in low vacuum (30 min, 535 °C, $4 \cdot 10^{-2}$ Pa). c) ZnO whiskers after 12 nm Ga deposition and subsequent annealing in high vacuum (30 min, 535 °C, $7 \cdot 10^{-4}$ Pa). d) Ga $2p_{3/2}$ peak obtained ex-situ by XPS (after exposure to atmospheric conditions) for the sample shown in (c). e) High resolution TEM image of the sample shown in (c), taken close to the sidewall (top of the image). The ZnO crystal planes are clearly visible even at the sidewall surface, with no indications of a surface gallium oxide layer. The contrast changes are due to variations in the sample thickness. The scale bars in a)–c) are 200 nm; in e) it is 1 nm.

Upon the Ga deposition (nominal thickness of 12 nm; calibrated with a crystal quartz thickness monitor), the ZnO whiskers are decorated with characteristic gallium droplets (see ex-situ SEM in Fig. 2a). For all the samples that follow, the Ga diffusion step (i.e. the annealing step promoting the Ga diffusion) was performed immediately after the Ga deposition under vacuum to avoid Ga oxidation. This is necessary for Ga interdiffusion into ZnO, as the formation of thermally stable gallium oxide would prevent Ga diffusion. Here, it is worth noting that Ga affinity for oxygen is very high, so the annealing step has to be performed in a very high vacuum. At pressures higher than 10^{-4} Pa the gallium droplets oxidise and the amount of Ga available for diffusion is very low (see Fig. 2b, showing oxidised Ga droplet shells after the diffusion annealing step). For the chamber pressure lower than $7 \cdot 10^{-4}$ Pa, the annealing at

535 °C for 30 minutes resulted in full consumption of the Ga droplets, as documented in Fig. 2c. The presence of gallium in this sample was confirmed by ex-situ XPS (Fig. 2d). The appearance of the whisker sidewalls changed significantly upon the diffusion step – the surface gets rough, exhibiting etch pits (see Fig. 2c). This phenomenon is discussed in section 3.3. The ex-situ XPS analysis of the sample shows gallium-related peaks at binding energies that are shifted with respect to metallic gallium (see e.g. the Ga $2p_{3/2}$ peak in Fig. 2d), suggesting the Ga valence close to Ga^{3+} state in Ga_2O_3. TEM analysis (Fig. 2e) confirms that the whiskers are defect-free ZnO single crystals up to their very surface; the value of 0.26 nm in [0001] direction corresponds to the ZnO bi-layer spacing in the ZnO crystal. Additionally, a fast Fourier transformation analysis of images taken on a larger area along the whisker sidewall shows only a single pattern assigned to ZnO (see the Supplementary information, Fig. S1). The presence of e.g. a Ga_2O_3 surface layer or inclusions within the ZnO lattice is therefore excluded. TEM imaging suggests that the gallium atoms have been incorporated into the ZnO lattice and that the XPS signal comes from gallium bound to oxygen atoms in the ZnO lattice rather than gallium oxide.

Fig. 3: Cross-sectional STEM EDS map of gallium in V_O-rich (a) and V_O-poor (b) Ga-diffused whisker. The scale bars, 200 nm. c) Gallium EDS depth-profiles for V_O-rich (blue) and V_O-poor (red) whisker. The profiles are recorded along the coloured dashed lines shown in a) and b). The line spectra are integrated over an area indicated by the dotted lines of the same colour. The spectra represent depth-profiles perpendicular to whisker sidewall facets. The dashed lines show the Ga concentration profiles extracted from the diffusion model for the V_O-rich and V_O-poor whisker, respectively. The surface-influenced regions are not considered in the diffusion model (see the text for details).

To investigate the Ga concentration profiles after the diffusion step, a pair of V_O-rich and V_O-poor samples was prepared. After the pre-annealing step in high vacuum or H_2O_2 (300 °C, 30 min) and subsequent Ga deposition (9 nm), the samples were annealed at 480 °C for 75 min to ensure Ga diffusion. At the end of the process, the in-situ SEM inspection showed similar whisker morphology as in Fig. 2c, yet the etch pits seem shallower, presumably due to lower annealing temperature. Then, we prepared cross-sectional TEM lamellae out of these whiskers using the Xe focused ion beam. The cross-sections were analysed with STEM EDS – see the gallium concentration maps in Fig. 3a,b for the V_O-rich and V_O-poor whisker, respectively. The contour of the whiskers is clearly visible as the Ga concentration is the highest near the whisker surface. Whereas the V_O-rich sample shows a gradual decrease in Ga concentration towards the

whisker centre (see Fig. 3a), gallium clustering is observed in the vicinity of the surface of the V_O-poor whisker despite the long annealing (Fig. 3b). This suggests that not all Ga was consumed within the annealing step.

To assess the penetration depth of gallium in each sample, Ga concentration profiles were measured in the cluster-free areas of both whiskers, along the coloured lines indicated in Fig. 3a,b. Knowing ZnO whisker geometry with respect to the growth substrate and the lamella orientation allows to obtain representative Ga depth profiles perpendicular to a whisker sidewall. Both samples show a maximum corresponding to a surface-affected area followed by a decreasing Ga concentration, detectable more than 100 nm below the surface. Note that the initial amount of deposited gallium was not identical for the two whiskers inspected due to the different geometry of whisker sidewalls with respect to the incoming gallium flux. Although the surface Ga concentration on the V_O-rich whisker is lower, it penetrates deeper into the whisker, suggesting dissimilar diffusion kinetics in the samples. Therefore, the measured concentration profiles were fitted with a diffusion model (see the dashed lines in Fig. 3c) to assess and compare the diffusion parameters of Ga in the V_O-rich and V_O-poor ZnO whiskers. In the model, gallium concentration is considered as a solution of Fick's second law for the limited-source diffusion in 1D case:

$$\varphi(x,t) = \frac{Q}{\sqrt{2Dt} \cdot \sqrt{2\pi}} \cdot e^{-\frac{x^2}{2(\sqrt{2Dt})^2}} \, , \tag{Eq. 1}$$

with the x axis oriented perpendicular to the surface, t representing the annealing duration, D being the diffusion coefficient of Ga in ZnO for a given annealing temperature and Q representing the initial amount of gallium deposited on the whisker facet. Then, the diffusion length may be defined as $\sqrt{2Dt}$. The diffusion length derived from the curves in Fig. 3c differs significantly between the two samples, being 71 nm for the V_O-rich whisker and 48 nm for the V_O-poor one. The diffusion coefficient D varies accordingly; $5.7 \cdot 10^{-19}$ m$^2 \cdot$s^{-1} and $2.6 \cdot 10^{-19}$ m$^2 \cdot$s^{-1} for the V_O-rich and V_O-poor whisker, respectively. The fitting procedure considered the inner

tail of the measured profiles only, disregarding the very surface area (due to excess surface Ga and the clustering effects).

3.3 Ga-diffused whiskers – melt-back etching

Our interest turns now to explaining the formation of the etch pits and Ga clusters below the surface, as seen in Fig. 2c and 3b, respectively. To unravel the mechanism behind the etch-pit formation, we have performed in-situ electron microscopy and X-ray photoelectron spectroscopy experiments during the Ga diffusion step on Ga covered ZnO samples, pre-annealed in high vacuum. Fig. 4a shows an image sequence taken on a whisker top facet during its in-situ annealing inside the microscope. A shadowing effect from a nearby whisker (not in the image) during the Ga deposition allows simultaneous imaging of an area with deposited Ga droplets and gallium-free ZnO surface. The image sequence clearly shows that the gallium droplets promote a selective etching of the ZnO surface – the etch pits are formed only at the locations of the Ga droplets. No etch pits are observed on the gallium-free areas.
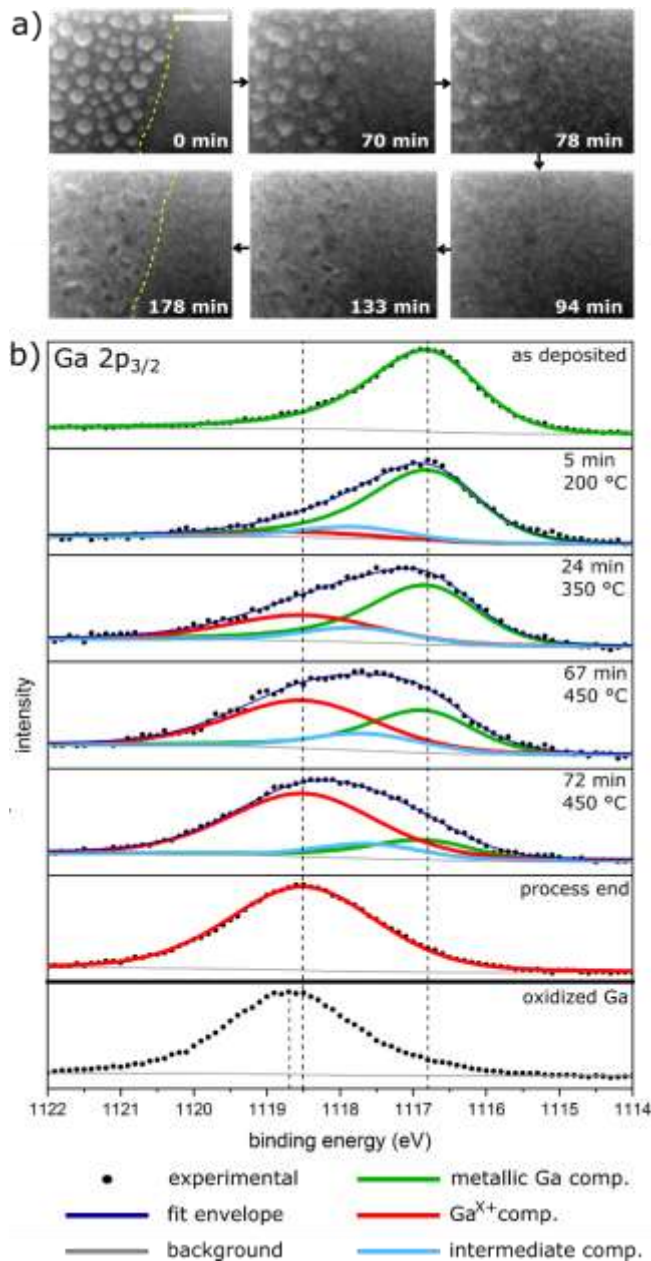
Fig. 4: In-situ microscopy and spectroscopy during the Ga diffusion step. The experiments were conducted in two different instruments, SAM (a) and XPS connected to the complex ultrahigh vacuum system (b). The temperature ramps differ for each experiment and, hence, the timestamps cannot be directly compared between the two experiments. (a) A real-time image sequence taken during in-situ annealing of the sample inside the electron microscope. The sample temperature during annealing reached 450 °C. The yellow line marks the shadow contour separating the area with/without deposited gallium. The scale bar is 200 nm. b) XPS analysis of the Ga $2p_{3/2}$ peak during in-situ annealing of the sample. The very bottom peak shows an ex-situ oxidised Ga/ZnO sample for comparison. The dashed vertical lines mark the peak position of the metallic Ga component (1116.65 eV), the higher-valence Ga component (1118.5 eV, labelled as Ga^{X+}) and the oxidised Ga component (1118.7 eV).

The in-situ XPS analysis allows collecting data that are not compromised by exposure to ambient atmosphere, which can severely complicate the peak deconvolution and interpretation. The as-deposited Ga on ZnO exhibits a single-component Ga $2p_{3/2}$ peak (for deconvolution details, see the Supplementary information) assigned to metallic Ga (see Fig. 4b). At the end of the diffusion-annealing process, the Ga $2p_{3/2}$ peak changes its shape and position. It can be fitted by a single Voigt-shape component with a larger full-width at half-maximum (FWHM), being indicative of Ga in a higher valence state with no metallic Ga present. Interestingly, this component (labelled as Ga^{X+} in Fig. 4b) exhibits larger FWHM and an 0.2 eV shift towards lower binding energies compared to Ga oxidised in ambient atmosphere (see the Supplementary information). Indeed, this Ga^{X+} component can only be related to the Ga–O bond, which is confirmed by the O 1s peak evolution. The O 1s peak gets broader after the process due to a new component at the higher-energy side (see the Supplementary information, Fig. S2), leading to a conclusion that this new O 1s peak component is related to the Ga–O bond as well. Further, the Ga $2p_{3/2}$ peak evolution documented in Fig. 4b shows another remarkable detail. During the process, the Ga $2p_{3/2}$ peak cannot be fitted by the two components (metallic and higher-valence-state Ga) only; a third component is necessary (labelled as "intermediate" in Fig. 4b). This component is only present during the annealing step and any hypothesis of its origin would be highly speculative at this point. However, it clearly represents an intermediate state of Ga atoms diffusing through the ZnO lattice.

4. Discussion

The Ga depth profiles shown in Fig. 3c indicate that the presence of crystal defects arising from annealing of ZnO in high vacuum conditions (presumably oxygen vacancies) promotes Ga interdiffusion into the ZnO lattice. In Fig. 4b, the XPS data taken in-situ after the diffusion step indicate that the valence state of diffused Ga differs from the native Ga oxides [23, 24], being shifted to lower binding energies with respect to Ga^{3+} in native Ga$_2$O$_3$. This behaviour is

consistent with available XPS data on other transparent conductive oxides (Sn-doped indium oxide [20], Al-doped zinc oxide [25]), which also show shifts of the dopant-related peaks towards lower binding energies. The lower valence of Ga measured by XPS suggests that the presence of oxygen vacancies is also beneficial for Ga incorporation into the ZnO lattice, allowing Ga to occupy zinc sites within the lattice with a valence shifted closer to Ga^{2+}.

The formation of etch pits during the diffusion step is surprising, given that it has not been observed in a similar Al–ZnO system [26]. However, there are indirect indications in the literature that such an effect might exist in the Ga–ZnO system. Ga presence during the growth of ZnO whiskers strongly influences the sidewall morphology, preferring different crystallographic orientations over commonly observed ones for pure ZnO growth [5]. Moreover, rough sidewalls (in comparison to Sn- and Al-doped ZnO) of Ga-doped ZnO whiskers were also reported previously [27]. The in-situ microscopy (Fig. 4a) clearly revealed that the etch-pit formation is related to Ga droplets, which locally etch the ZnO surface. Such an effect, called melt-back etching, is well known from GaN epitaxy on silicon, where excess Ga causes etching of the silicon substrate [11, 12]. For that particular material system, the mechanism remains not fully revealed yet. However, in the case of Ga–ZnO, the explanation based on our data is straightforward: The gallium droplets decompose ZnO and consume Zn underneath and, thus, sink into the whisker while continuously losing Ga because of its out-diffusion into the ZnO crystal. Supporting this conclusion, a spontaneous uptake of zinc by Ga-containing compounds has been reported earlier [19, 28, 29]. The dissolution of zinc in liquid Ga is possible even at very low temperatures, given a low eutectic point of the Ga–Zn melt [30]. The excess zinc easily evaporates from the droplet due to its high vapour pressure.

If the consumption of Ga droplet is not finished (which is favourable for the V_O-poor samples due to slower Ga diffusion rates, see Fig. 3), liquid metallic Ga is left within the etched pit. This is observed in the STEM EDS image in Fig. 3b. The pathway of zinc atoms in this process is

through solid, liquid and vapour phases (SLV), thus being similar to the SLV mechanism reported earlier for other material systems [31].

Similarly to the GaN–Si system, the melt-back etching plays a detrimental role in diffusion doping of ZnO with Ga and has to be avoided. A possible way to minimise the melt-back etching of ZnO involves the combination of appropriate pre-annealing conditions (in-vacuum annealing promoting the Ga diffusion rate), temperature ramping and timescale of the process. Notably, while the Ga diffusion starts immediately after increasing the temperature (being already evident 5 minutes after starting the in-situ XPS experiments in Fig. 4b), the melt-back etching is observed with a significant delay (tens of minutes, see Fig. 4a). Such a difference suggests a larger kinetic barrier for zinc dissolution compared to Ga diffusion. Thus, the Ga diffusion step performed at lower temperatures than reported here could also be beneficial in order to suppress the melt-back etching.

5. Conclusion

We have shown that diffusion doping of ZnO whiskers results in the incorporation of Ga into the ZnO lattice. Gallium interdiffusion is faster and more homogeneous for the V_O-rich ZnO whiskers, compared with the V_O-poor ones. This clearly indicates different diffusion kinetics of Ga within V_O-rich and V_O-poor ZnO, although the modelling of the diffusion processes presented here shall rather be understood as a qualitative one. Additionally, the sharp boundaries between Ga clusters and ZnO material in the V_O-poor sample further indicate inhibition of Ga diffusion in the V_O-poor ZnO. Our experiments also revealed that the Ga–ZnO system suffers from the melt-back etching, being previously known from GaN–Si epitaxy. The results suggest a possible way to diminish the melt-back etching effect by in-vacuum pre-annealing and decreasing the temperature at which the Ga diffusion step is performed.

References

[1] A. Calzolari, A. Ruini, A. Catellani, Transparent Conductive Oxides as Near-IR Plasmonic Materials: The Case of Al-Doped ZnO Derivatives, ACS Phot. 1 (2014) 703−709. https://doi.org/10.1021/ph500118y

[2] S. Law, L. Yu, A. Rosenberg, D. Wasserman, All-semiconductor plasmonic nanoantennas for infrared sensing, Nano Lett. 13 (2013) 4569–4574. https://doi.org/10.1021/nl402766t

[3] M.A. Noginov, L. Gu, J.J. Livenere, G. Zhu, A.K. Pradhan, R. Mundle, M. Bahoura, Y.A. Barnakov, V.A. Podolskiy, Transparent conductive oxides: Plasmonic materials for telecom wavelengths, Appl. Phys. Lett. 99 (2011) 021101. https://doi.org/10.1063/1.3604792

[4] S.D. Ponja, S. Sathasivam, I.P. Parkin, C.J. Carmalt, Highly conductive and transparent gallium doped zinc oxide thin films via chemical vapor deposition, Sci. Rep. 10 (2020) 638. https://doi.org/10.1038/s41598-020-57532-7

[5] V. Sallet, C. Sartel, S. Hassani, C. Vilar, G. Amiri, A. Lusson, F. Jomard, P. Galtier, I. Lefebvre, C. Delerue, M.K. Hamza, B. Canut, B. Masenelli, Crystal Facet Engineering in Ga-Doped ZnO Nanowires for Mid-Infrared Plasmonics, Cryst. Growth Des. 18 (2018), 4287–4295. https://doi.org/10.1021/acs.cgd.8b00048

[6] J. Wallentin, M.T. Borgström, Doping of semiconductor nanowires, J. Mater. Res. 26 (2011) 2142–2156. https://doi.org/10.1557/jmr.2011.214

[7] W. Kim, L. Güniat, A. Fontcuberta i Morral, V. Piazza, Doping challenges and pathways to industrial scalability of III–V nanowire arrays, Appl. Phys. Rev. 8 (2021) 011304. https://doi.org/10.1063/5.0031549

[8] O. Hazut, B.-C. Huang, A. Pantzer, I. Amit, Y. Rosenwaks, A. Kohn, C.-S. Chang, Y.-P. Chiu, R. Yerushalmi, Parallel p–n Junctions across Nanowires by One-Step Ex Situ Doping, ACS Nano 8 (2014) 8357-8362. https://doi.org/10.1021/nn502855k

[9] J. Resasco, N.P. Dasgupta,; J.R. Rosell, J. Guo, P. Yang, , J. Am. Chem. Soc. 136, (2014) 10521-10526. https://doi.org/10.1021/ja505734s

[10] Z. Sun, O. Hazut, B.-C. Huang, Y.-P. Chiu, C.-S. Chang, R. Yerushalmi, L.J. Lauhon, D.N. Seidman, Dopant Diffusion and Activation in Silicon Nanowires Fabricated by ex Situ Doping: A Correlative Study via Atom-Probe Tomography and Scanning Tunneling Spectroscopy, Nano Lett. 16 (2016) 4490-4500. https://doi.org/10.1021/acs.nanolett.6b01693

[11] H. Ishikawa, K. Yamamoto, T. Egawa, T. Soga, T. Jimbo, M. Umeno, Thermal stability of GaN on (111) Si substrate, J. Cryst. Growth 189/190 (1998) 178–182. https://doi.org/10.1016/S0022-0248(98)00223-1

[12] Y. Zheng, M. Agrawal, N. Dharmarasu, K. Radhakrishnan, S. Patwal, A study on Ga–Si interdiffusion during (Al)GaN/AlN growth on Si by plasma assisted molecular beam epitaxy, Appl. Surf. Sci. 481 (2019) 319–326. https://doi.org/10.1016/j.apsusc.2019.03.046

[13] S. Vallejos, N. Pizúrová, I. Gràcia, C. Sotelo-Vazquez, J. Čechal, C. Blackman, I. Parkin, C. Cané, ZnO rods with exposed {100} facets grown via a self-catalyzed vapor−solid mechanism and their photocatalytic and gas sensing properties, ACS Appl. Mater. Interfaces 8 (2016) 33335–33342. https://doi.org/10.1021/acsami.6b12992

[14] J. Zúñiga-Pérez, V. Consonni, L. Lymperakis, X. Kong, A. Trampert, S. Fernández-Garrido, O. Brandt, H. Renevier, S. Keller, K. Hestroffer, M.R. Wagner, J.S. Reparaz, F. Akyol, S. Rajan, S. Rennesson, T. Palacios, G. Feuillet, Polarity in GaN and ZnO: Theory, measurement, growth, and devices, Appl. Phys. Rev. 3 (2016) 041303. https://doi.org/10.1063/1.4963919

[15] A. El-Shaer, A. Che Mofor, A. Bakin, M. Kreye, A. Waag, High-quality ZnO layers grown by MBE on sapphire, Superlattices and Microstruct. 38 (2005), 265–271. https://doi.org/10.1016/j.spmi.2005.08.025

[16] M. Kolíbal, T. Pejchal, T. Vystavěl, T. Šikola, The Synergic Effect of Atomic Hydrogen Adsorption and Catalyst Spreading on Ge Nanowire Growth Orientation and Kinking, Nano Lett. 16 (2016), 4880–4886. https://doi.org/10.1021/acs.nanolett.6b01352

[17] A. Janotti, C.G. Van de Walle, Fundamentals of zinc oxide as a semiconductor, Rep. Prog. Phys. 72 (2009) 126501. https://doi.org/10.1088/0034-4885/72/12/126501

[18] H. Rotella, Y. Mazel, S. Brochen, A. Valla, A. Pautrat, C. Licitra, N. Rochat, C. Sabbione, G. Rodriguez, E. Nolot, Role of vacancy defects in Al doped ZnO thin films for optoelectronic devices, J. Phys. D: Appl. Phys. 50 (2017) 485106. https://doi.org/10.1088/1361-6463/aa920b

[19] J. Wang, H. Sun, Y. Sheng, L. Yang, F. Gao, Y. Yin, Z. Hu,Q. Wan, R. Zhang, Y. Zheng, Yi Shi, Surface-diffusion enhanced Ga incorporation in ZnO nanowires by oxygen vacancies, Appl. Surf. Sci. 361 (2016) 221–225. https://doi.org/10.1016/j.apsusc.2015.11.177

[20] J.C.C. Fan, J.B. Goodenough, X-ray photoemission spectroscopy studies of Sn-doped indium-oxide films, J. Appl. Phys. 48 (1977), 3524–3531. https://doi.org/10.1063/1.324149

[21] H. Idriss, On the wrong assignment of the XPS O1s signal at 531–532 eV attributed to oxygen vacancies in photo- and electro-catalysts for water splitting and other materials applications, Surf. Sci. 712 (2021), 121894. https://doi.org/10.1016/j.susc.2021.121894

[22] B. Ha, H. Ham, C.J. Lee, Photoluminescence of ZnO nanowires dependent on O_2 and Ar annealing, J. Phys. Chem. Solids 69 (2008) 2453–2456. https://doi.org/10.1016/j.jpcs.2008.04.041

[23] M.J. Regan, H. Tostmann, P.S. Pershan, X-ray study of the oxidation of liquid-gallium surfaces, Phys. Rev. B 55 (1997) 10786–10790. https://doi.org/10.1103/PhysRevB.55.10786

[24] C.Y. Su, P.R. Skeath, I. Lindau, W.E. Spicer, Photoemission studies of room-temperature oxidized Ga surfaces, Surf. Sci. 118 (1982) 248–256.

[25] M. Chen, X. Wang, Y.H. Yu, Z.L. Pei, X.D. Bai, C. Sun, R.F. Huang, L.S. Wen, X-ray photoelectron spectroscopy and auger electron spectroscopy studies of Al-doped ZnO films, Appl. Surf. Sci. 158 (2000) 134–140. https://doi.org/10.1016/S0169-4332(99)00601-7

[26] Y. Gao, M. Iachella, E. Mattson, A. T. Lucero, J. Kim, M. D. Rouhani, Y. Chabal, C. Rossi, A. Estève, Al Interaction with ZnO Surfaces, J. Phys. Chem. C 122 (2018) 17856-17864. https://doi.org/10.1021/acs.jpcc.8b04952

[27] S.Y. Bae, C.W. Na, J.H. Kang, J. Park, Comparative Structure and Optical Properties of Ga-, In-, and Sn-Doped ZnO Nanowires Synthesized via Thermal Evaporation, J. Phys. Chem. B 109 (2005) 2526–2531. https://doi.org/10.1021/jp0458708

[28] J.B. Park, Y.T. Chun, Y.B. Lee, J.I. Sohn, W.-K. Hong, Defect-mediated modulation of optical properties in vertically aligned ZnO nanowires via substrate-assisted Ga incorporation, Nanotechnology 26 (2015) 145202. https://doi.org/10.1088/0957-4484/26/14/145202

[29] J. Wang, H. Sun, Y. Sheng, F. Gao, Y. Yin, Y. Li, L. Pan, Y. Zheng, Y. Shi, T. Sekiguchi, Spontaneous Ga incorporation in ZnO nanowires epitaxially grown on GaN substrate, Phys. Status Solidi RRL 9 (2015) 466–469. https://doi.org/10.1002/pssr.201510229

[30] J. Dutkiewicz, Z. Moser, L. Zabdyr, D.D. Gohil, T.G. Chart, I. Ansara, C. Girard, The Ga-Zn (Gallium-Zinc) System, Bull. Alloy Phase Diagr. 11 (1990) 77–82.

[31] M. O'Toole, J.J. Boland, A solid-liquid-vapor mechanism for anisotropic silicon etching, Appl. Phys. Lett. 93 (2008) 263107. https://doi.org/10.1063/1.3055606.